Supporting Information

Enhancing bifunctional electrocatalytic performance of electrodeposited medium entropy alloy films by configurational entropy engineering

Pratibha Kushwah, Pushpesh Pathak, Perumal Alagarsamy, and Ananthakrishnan Srinivasan*

Department of Physics, Indian Institute of Technology Guwahati, Guwahati,

Assam – 781039, India.

*asrini@iitg.ac.in

1. Experimental section

Electrodeposition

Co-Fe-Sn and Co-Fe-Ni-Sn medium entropy alloy (MEA) films were electrodeposited on 10 ×10 mm^2 Cu substrates using a prepared electrolyte. The electrolyte was formulated by dissolving the calculated amounts of metal salt precursors and additives in 250 mL of deionized water. The concentrations of the metal salts and additives employed for the deposition of the alloy films are summarized in Table S1.

Table S1. Concentration of metal salts and additives used to prepare the alloy films.

Chemicals	Film composition				
	CFS	CFNS-1	CFNS-2	CFNS-3	CFNS-4
Ascorbic acid	1.0000 g	1.0000 g	1.0000 g	1.0000 g	1.0000 g
$CoSO_4.7H_2O$	5.1306 g	4.2465 g	3.8308 g	2.6014 g	3.0000 g
$FeSO_4.7H_2O$	4.5395 g	2.9266 g	2.9266 g	2.9266 g	2.9266 g
$NiSO_4.6H_2O$	0 g	6.0000 g	8.0000 g	13.7500 g	13.7500 g
$SnSO_4.7H_2O$	0.4078 g	0.1966 g	0.2890 g	0.20933 g	0.1964 g
Boric acid	4.6380 g	4.6380 g	4.6380 g	4.6380 g	4.6380 g
NaCl	4.1160 g	4.1160 g	4.1160 g	4.1160 g	4.1160 g
Sodium gluconate	30.000 g	30.000 g	30.000 g	30.000 g	30.000 g
Peptone	0.0050 g	0.0050 g	0.0050 g	0.0050 g	0.0050 g

EDS spectra and elemental maps of MEA films:

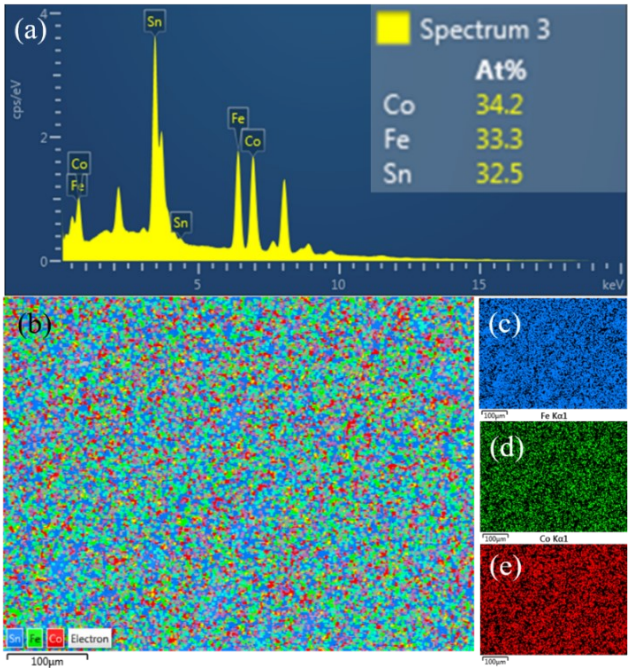

Figure S1. (a) Typical EDS spectra of CFS alloy, elemental map of (b) Co:Fe:Sn:34.2:33.3:32.5, (c) Sn, (d) Fe, (e) Co film.

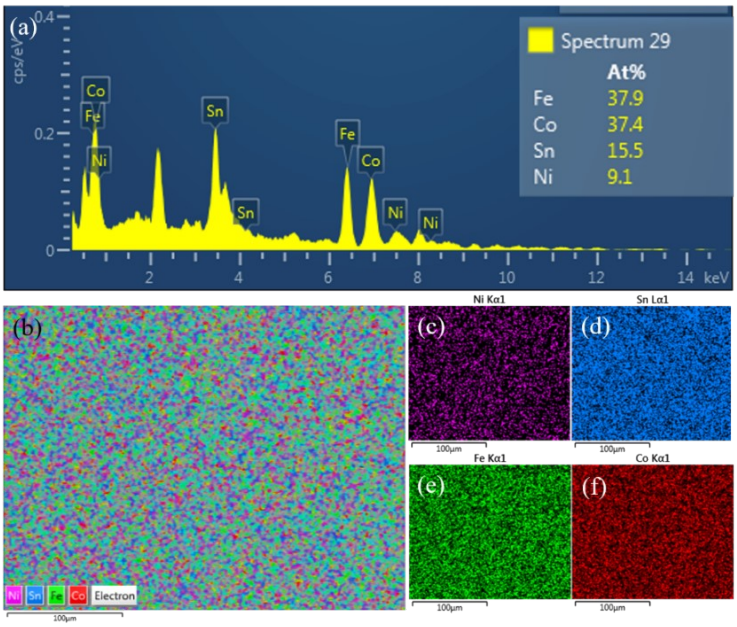

Figure S2. (a) Typical EDS spectra of CFSN-1 alloy, elemental map of (b) Co:Fe:Sn:Ni:37.4:37.9:15.5:9.1, (c) Ni, (d) Sn, (e) Fe, and (f) Co film.

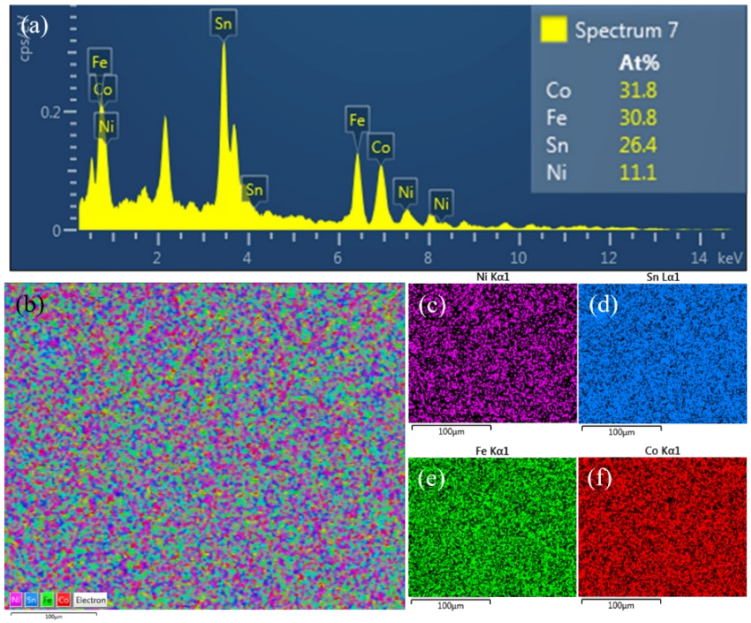

Figure S3. (a) Typical EDS spectra of CFSN-2 alloy, elemental map of (b) Co:Fe:Sn:Ni:31.8:30.8:26.4:11.1, (c) Ni, (d) Sn, (e) Co, and (f) Fe film.

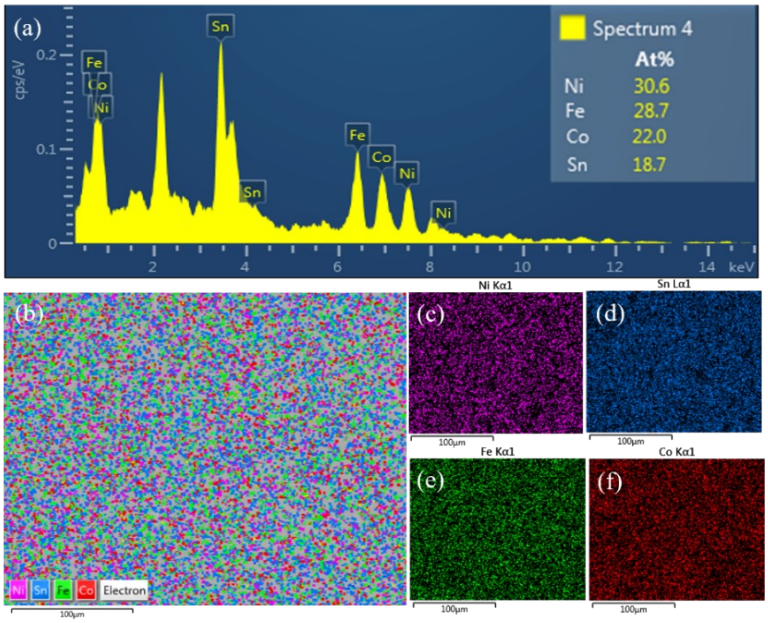

Figure S4. (a) Typical EDS spectra of CFSN-3 alloy, elemental map of (b) Co:Fe:Ni:Sn::22.0:28.7:30.6:18.7, (c) Ni, (d) Sn, (e) Fe, and (f) Co film.

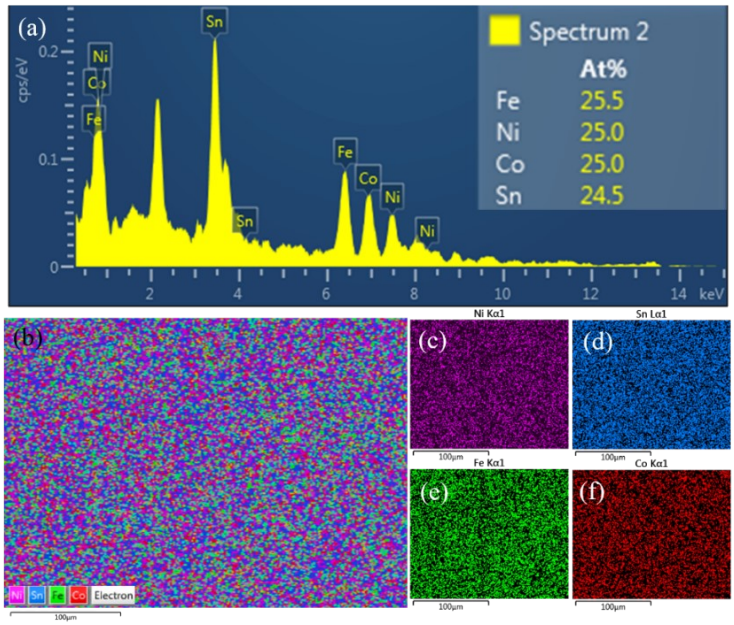

Figure S5. (a) Typical EDS spectra of CFSN-4 alloy, elemental map of (b) Co:Fe:Ni:Sn:25.0:25.5:25.0:24.5, (c) Ni, (d) Sn, (e) Fe, and (f) Co film.

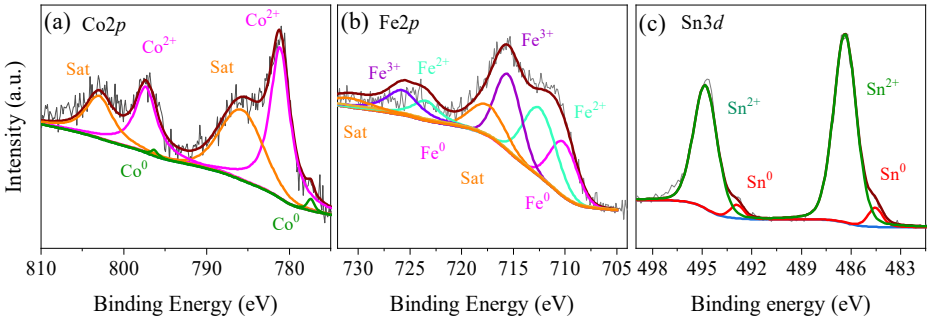

Figure S6. XPS spectra of the CFS MEA film showing the deconvoluted core-level peaks of (a) Co 2*p*, (b) Fe 2*p*, and (c) Sn 3*d*.

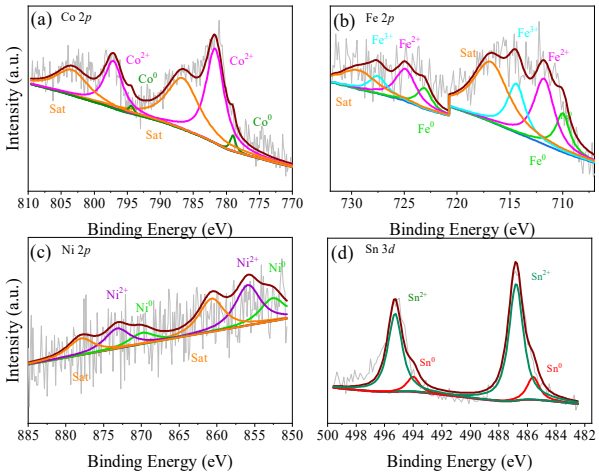

Figure S7. XPS spectra of the CFNS-1 MEA film showing the deconvoluted core-level peaks of (a) Co 2*p*, (b) Fe 2*p*, (c) Ni 2*p*, and (d) Sn 3*d*.

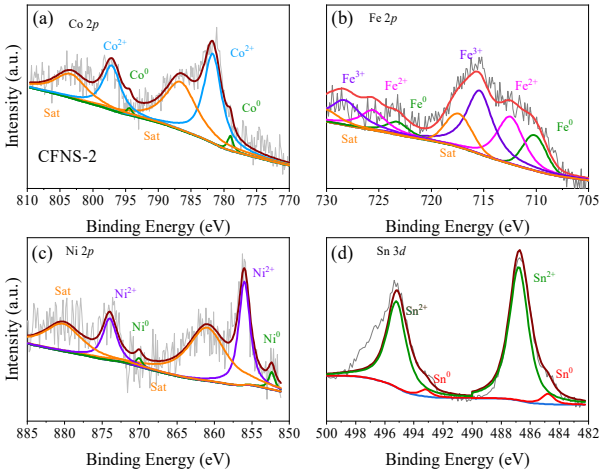

Figure S8. XPS spectra of the CFNS-2 MEA film showing the deconvoluted core-level peaks of (a) Co 2*p*, (b) Fe 2*p*, (c) Ni 2*p*, and (d) Sn 3*d*.

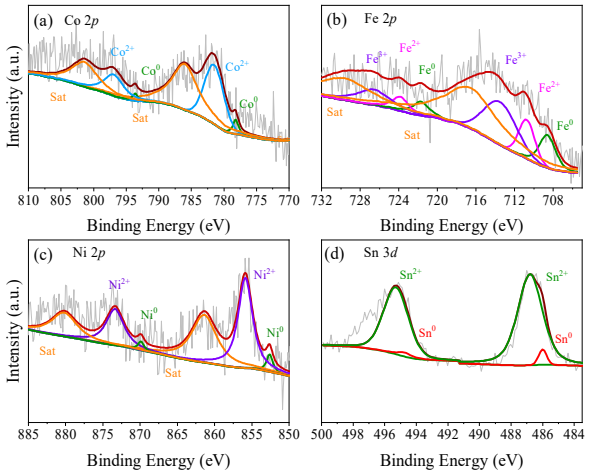

Figure S9. XPS spectra of the CFNS-2 MEA film showing the deconvoluted core-level peaks of (a) Co 2*p*, (b) Fe 2*p*, (c) Ni 2*p*, and (d) Sn 3*d*.

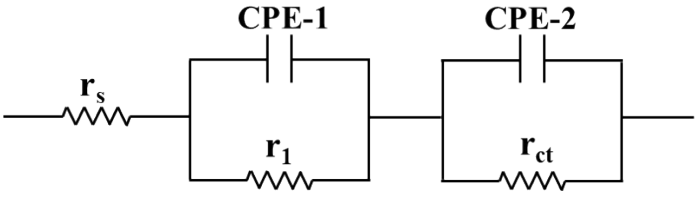

Figure S10. Equivalent circuit used for EIS analysis.

The long-term stability of the catalysts toward the HER was investigated using chronoamperometry at different current densities over a duration of 10 h (Figure S11). All samples exhibit stable current density responses over time, indicating good electrochemical durability under continuous HER operation.

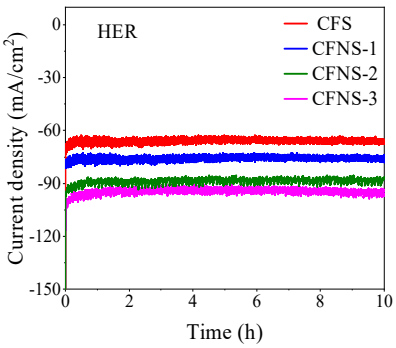

Figure S11. HER chronoamperometry-based stability curve of CFS, CFSN-1, CFSN-2, and CFSN-3 MEA films.

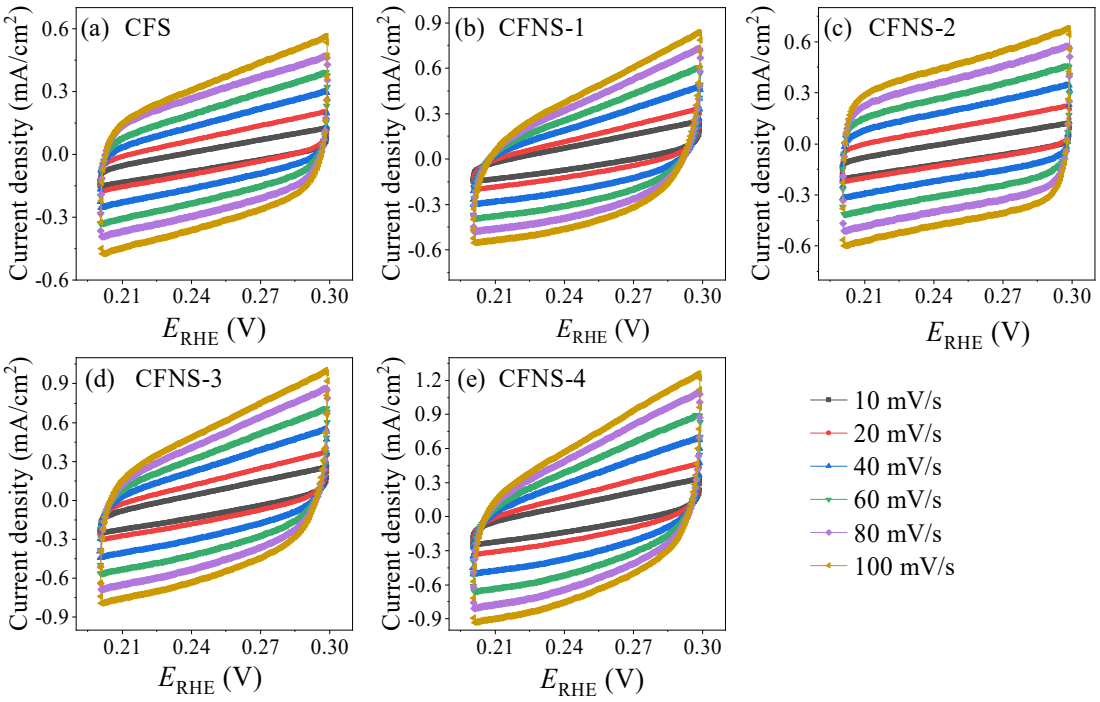

Figure S12. CV scans recorded in the non-Faradic region for (a) CFS, (b) CFNS-1, (c) CFNS-2, (d) CFNS-3, and (e) CFNS-4 MEA films.

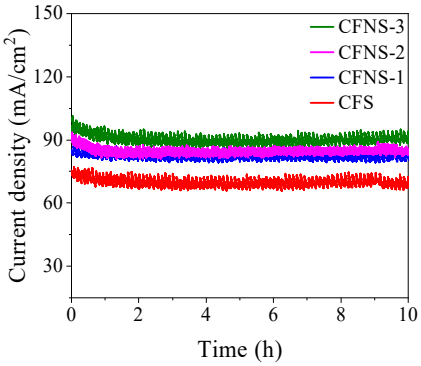

Figure S13. OER chronoamperometry-based stability curve of CFS, CFSN-1, CFSN-2, and CFSN-3 MEA films.

To understand the effect of catalytic activity on the structural changes of the MEA films, Ex-situ XRD patterns were recorded before and after HER and OER measurements. Comparison of Figure S14(a) before catalytic activity, (b) after HER, and (c) after OER clearly show that there are no additional peaks in the XRD patterns recorded before and after the electrochemical studies. This confirms the absence of any significant structural changes in the MEA films after the electrochemical studies.

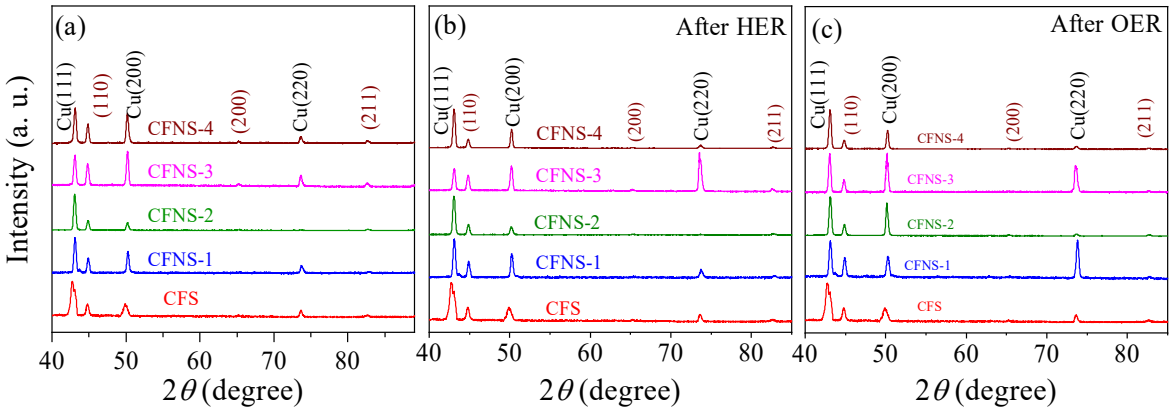

Figure S14. XRD patterns of CFS, CFNS-1, CFNS-2, CFNS-3, and CFNS-4 after (a) before catalytic activity (b) HER and (c) OER, demonstrating the structural stability of the bcc-like phase under electrochemical conditions.

Table S2. Comparison of overpotential at 10 mA/cm^2 (η_{10}), various alloy electrocatalysts for HER in 1.0 M KOH.

Catalyst	Overpotential (mV)	Tafel slope (mV/dec)	Reference
CFNS-4	100.3	46.7	This work
CFNS-3	114.6	52.8	
CFNS-4	123.7	54.4	
CFNS-3	133.8	64.3	
CFS	154.8	71.2	
NiCoCr	205	159	[1]
NiCoV	232	169	
NiCo(CrV)	119	105	
NiCo(CrV) - 1 μm	87	96	
FeCoNi	333	305.8	[2]
FeCoNiPt	144	167.1	
FeCoNiRu	316	216.1	
FeCoNiPtRu	321	159.4	
NiMnGaCu (A)	230	200	[3]
NiMnGaCu (M)	150	193	
CuCrP	306	136	[4]
CuCrFeP	334	158	
CuCrFeNiP	263	129	
CuCrFeNiCoP	195	118	
NiFeMoCoCr	172	66	[5]

Table S3. Charge transfer resistance values of MEA films in HER and OER

Sample Id	r_{ct} (Ω) for HER	r_{ct} (Ω) for OER
CFS	11.6	20.867
CFNS-1	9.2	16.839
CFNS-2	6.1	12.477
CFNS-3	4.5	8.5583
CFNS-4	3	6.6877

Table S4. Comparison of overpotential at 10 mA/cm^2 (η_{10}), various alloy electrocatalysts for OER in 1.0 M KOH.

Catalyst	Overpotential (mV)	Tafel slope (mV/dec)	Reference
CFNS-4	319.7	55.5	This work
CFNS-3	326.5	56.3	
CFNS-4	338.1	56.7	
CFNS-3	349.7	66.1	
CFS	363.7	68.7	
NiCoCr	369	82	[1]
NiCoV	361	75	
NiCo(CrV)	350	72	
NiCo(CrV) - 1 µm	320	69	
FeCoNi	356	57.3	[2]
FeCoNiPt	345	52.2	
FeCoNiRu	314	51	
FeCoNiPtRu	331	50	
NiMnGaCu (A)	200	176	[3]
NiMnGaCu (M)	280	126	
CuCrP	383	111.4	[4]
CuCrFeP	376	94.9	
CuCrFeNiP	296	108.6	
CuCrFeNiCoP	270	70.7	

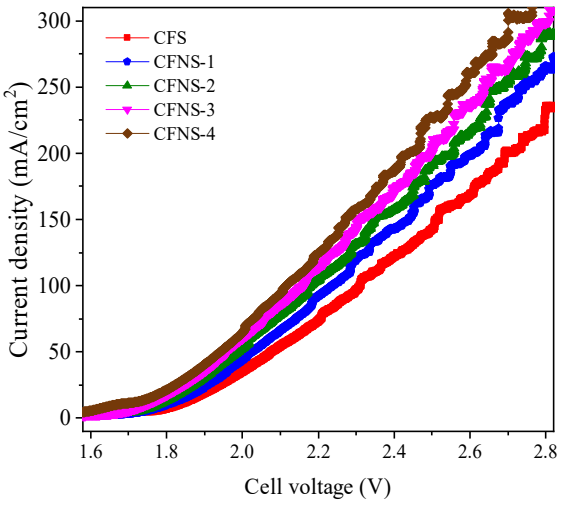

Figure S15. LSV curve for overall water splitting of all the MEA films recorded using a two-electrode configuration.

References

[1] S. Ahmad, M. Egilmez, W. Abuzaid, F. Mustafa, A. M. Kannan, A. S. Alnaser, *Int. J. Hydrog. Energy* 52 (2024) 1428-1439.

[2] M. Geng, Y. Zhu, J. Guan, R. Zhang, Q. Zou, L. Wang, B. Guo, M. Zhang, *J. Alloys Compd*. 1005 (2024) 176180.

[3] M. Tiwari, P. K. Bhartiya, N. Bangruwa, S. K. Sarkar, D. Mishra, *ACS Appl. Mater. Interfaces* 16 (2024) 69398–69409.

[4] T. Zhang, J. Li, B. Zhang, G. Wang, K. Jiang, Z. Zheng, J. Shen, *J. Alloys Compd.* 969 (2023) 172439.

[5] G. Zhang, K. Ming, J. Kang, Q. Huang, Z. Zhang, X. Zheng, and X. Bi, *Electrochim. Acta* 279 (2018) 19-23.

******